NEOPLASIA
www.neoplasia.com
Volume 11 Number 5 May 2009 pp. 509–519 509

Inhibition of Breast Cancer Metastasis and Angiogenesis by Antiosteopontin Single-Chain Fv-Fc Fusion Protein[1]

Ling Peng*,†, Yajun Guo†, Yun Zhou‡, Jianxin Dai† and Hao Wang†

*Department of Medicinal Oncology, Jinling Hospital, Medical School of Nanjing University, Nanjing, Jiangsu Province 210002, People's Republic of China; †Shanghai International Joint Cancer Institute, Second Military Medical University, Shanghai 200433, People's Republic of China; ‡Zhejiang Food and Drug Administration, Hangzhou, Zhejiang Province 310012, People's Republic of China

Abstract

Osteopontin (OPN) is associated with many diseases, and its role in tumor growth and metastasis has been studied in breast cancers. Previous studies have described anti-OPN antibodies that could inhibit tumor cell adhesion and invasion *in vitro*, but until now, there are no systematic studies on antitumor effects of anti-OPN antibodies *in vivo*. In the present study, we have raised several anti-OPN single-chain variable fragments from phage antibody library and expressed them as single-chain variable fragment–constant region fragment fusion proteins in Chinese hamster ovary cells. Of them, two antibodies (1A12 and 2H8) were able to inhibit MDA-MB-435s breast cancer cell attachment, invasion, migration, and colony formation in soft agar. Furthermore, 1A12 and 2H8 inhibited the antiapoptotic and prosurvival functions of OPN in human umbilical vein endothelial cell. In human umbilical vein endothelial cell capillary tube formation, chicken chorioallantoic membrane assay, and rabbit corneal micropocket assay, the two antibodies showed markedly inhibitory effects toward angiogenesis. We investigated antitumor effects of anti-OPN antibodies in nude mice by assessing xenograft tumor growth and lung metastasis potential. The results showed that the two antibodies were capable of delaying primary tumor growth and reducing spontaneous lung metastasis. Epitope mappings of these two anti-OPN antibodies were performed, and a new binding site of 1A12 was revealed. In summary, the present study has demonstrated the roles of anti-OPN antibodies in blocking the function of OPN, suggesting that they may have the potential to be developed for future clinical use.

Neoplasia (2009) 11, 509–519

Introduction

Tumor metastasis and angiogenesis are crucial steps in tumor development and dissemination. Several growth factors and cytokines play important roles in the adhesion, migration, invasion, and proliferation of tumor cells. Among them, osteopontin (OPN) has been linked with the regulation of metastatic spread of tumor cells by substantial data and associated with the metastatic phenotype of breast cancer [1].

Osteopontin is a secreted phosphorylated glycoprotein that has diverse physiological and pathological functions [2]. Its expression is associated with a variety of diseases or reactive states, including cancer, immune diseases, and vascular remodeling. The pivotal role of OPN in tumor metastasis has been highlighted by many researches [3,4]. Increased OPN expression is associated with tumor invasion, progression, and metastasis of breast, lung, prostate, and colon cancers. Studies have established a correlation between high levels of OPN protein expression and malignant invasion by demonstrating OPN expression within

Abbreviations: CAM, chorioallantoic membrane; Fc, constant region fragment; HUVEC, human umbilical vein endothelial cell; OPN, osteopontin; scFv, single-chain variable fragment

Address all correspondence to: Ling Peng, Department of Medicinal Oncology, Jinling Hospital, Medical School of Nanjing University, Nanjing, Jiangsu Province 210002, People's Republic of China. E-mail: dr.pengling@gmail.com

[1]This work was supported in part by the grants from National Natural Science Foundation of China, Shanghai Commission of Science and Technology and Ministry of Science and Technology of China (973 and 863 projects) as well as a special grant from Shanghai Pudong Bureau of Science and Technology of China.
Received 17 December 2008; Revised 16 February 2009; Accepted 18 February 2009

DOI 10.1593/neo.81622

tumor cells and in the surrounding stroma of numerous human cancers. Osteopontin is thought to exert its prometastatic effects by interacting with integrins and CD44 receptors. Because of its potential role in cancer cell motility, growth, and metastasis, OPN could be regarded as a candidate target in developing diagnostics and therapy for cancer.

It has been shown that OPN affects the behavior of breast cancer cells in a number of ways by influencing pathways involved in the control of cell adhesion, migration, and invasion. Incubation with mammary epithelial cells with OPN (native or recombinant) supports cell adhesion and induces cell migration and invasion [5]. Not only does OPN affect mammary epithelial cell migration but it also induces cell invasion through basement membrane Matrigel, when either added to the cells or endogenously increased by transfection. The degree of OPN-induced cell migration response may depend on the type of integrin receptors the cells express. The cells expressing $\alpha_v\beta_3$ integrin migrate better in response to OPN than those expressing only $\alpha_v\beta_5$ and β_1. MDA-MB-435s breast cancer cells express $\alpha_v\beta_3$ integrin, whereas some less malignant cell lines (MDA-MB-231, MCF-7, etc.) do not [6].

Osteopontin was regarded to be an important angiogenic factor in many processes [7]. Increased vascularity enhances the growth of primary tumors and provides a poor prognosis of tumor patients. It is known that both OPN and $\alpha_v\beta_3$ are expressed by endothelial cells during vascular remodeling [8]. *In vitro*, OPN has been found to promote endothelial cell survival [9] and to induce vascular endothelial growth factor (VEGF) expression by endothelial cells [10], and OPN might stimulate endothelial cell migration in cooperation with VEGF [11]. Furthermore, OPN might contribute to tumor growth and metastasis by inhibiting apoptosis of endothelial cells. Soluble OPN inhibits apoptosis of human umbilical vein endothelial cell (HUVEC) deprived of serum and growth factors and inhibits DNA fragmentation [12]. Osteopontin also supported tumor cell survival [13].

The production of OPN can contribute to the metastasis phenotype through autocrine and paracrine effects. Autocrine effects can modulate cell proliferation and survival, transforming benign tumor cells to malignant tumor cells [14]. Conversely, paracrine function of OPN can provide protection from cytotoxic macrophages by inhibiting the production of nitric oxide [15]. These functions may explain why tumor cells not expressing OPN are eliminated and provide the reason for tumor cell escape.

Osteopontin knockout mice showed impaired colony formation in soft agar and slower tumor growth *in vivo* compared with tumors in wild-type mice [16]. Several approaches including silencing of OPN expression at the messenger RNA (mRNA) and protein levels have been attempted. Silencing of OPN expression by small interfering RNA technology resulted in suppression of both *in vitro* and *in vivo* CT26 murine colon adenocarcinoma metastasis [17]. With the increasing interest in OPN as a potentially therapeutic target in different malignancies, we constructed human OPN-immunized phage antibody library to generate anti-OPN antibodies and to study their functions. We investigated the antitumor effects of anti-OPN antibodies *in vitro* and *in vivo*. Our findings indicate that anti-OPN antibodies inhibit MDA-MB-435s cell attachment, invasion, migration, and colony formation in soft agar. The antibodies inhibit angiogenesis and antiapoptotic functions of OPN. *In vivo* xenograft models of MDA-MB-435s breast cancer have shown that anti-OPN antibodies have antitumor effects *in vivo*. These results demonstrate that anti-OPN antibodies may possess therapeutic activity for the treatment of tumors that are dependent on OPN signaling for growth and metastasis.

Materials and Methods

Animals, Cell Lines, and Proteins

Female athymic nude mice, 4 to 6 weeks old, were obtained from the Animal Center, Chinese Academy of Sciences. MDA-MB-435s cells were obtained from the Cell Library of the Institute of Cellular Biology, Chinese Academy of Sciences. The HUVECs were purchased from Cascade Biologics (Portland, OR) and grown in the Medium 200 supplemented with low serum growth supplement (Cascade Biologics).

Recombinant human OPN protein was cloned from MDA-MB-435s cells and expressed in yeast vector pPICZαA and purified.

Generation of Anti-OPN Single-Chain Variable Fragment–Constant Region Fragment Fusion Proteins

Balb/c mice were immunized with recombinant human OPN and anti-OPN phage antibody library was constructed using pCANTAB5E phagemid vector (Amersham, Uppsala, Sweden). Biopanning was performed against the library, and positive clones were determined by monoclonal phage ELISA.

Single-chain variable fragment–constant region fragment (scFv-Fc) constructs were generated by cloning scFv into the pcDNA3.1(+) expression vector that contained the complementary DNA encoding the hinge-CH2-CH3 regions of the human immunoglobulin G1 heavy chain constant region (Fc). The scFv-Fc plasmids were stably transfected into Chinese hamster ovary cells. Supernatants were purified by Protein A chromatography and analyzed by Western blot analysis and competitive ELISA.

Cell Attachment Assay

The 96-well microtiter plates were coated with OPN, followed by treatment with 1% BSA for 1 hour at 37°C. To each well, 5×10^4 MDA-MB-435s cells were added in the presence or absence of various concentrations of anti-OPN antibodies. After incubation for 2 hours at 37°C, the medium was removed and washed twice with PBS gently. The adherent cells were fixed in 1% methanol, stained with 0.5% crystal violet, and lysed with 2% Triton X-100. The absorbance was measured at $OD_{595\,nm}$.

Cell Invasion Assay through Matrigel

Cell invasion was measured by 24-well Transwell system with polycarbonate filters of 8-μm pore size. The upper side was coated with Matrigel. After rehydration, 5×10^5 MDA-MB-435s cells with or without anti-OPN antibodies were added to the top chamber. To the lower chamber, 600-μl medium containing OPN was added. After 24 hours of incubation, the cells attached to the lower surface were stained and counted. Four high-power fields were counted for each well.

Scratch Wound Healing Assay

Monolayers of MDA-MB-435s cells were cultured to near confluence (>90%) in 12-well plates in triplicate. Streaks were made on the monolayer culture with 10-μl pipette tips. Experiment was performed with and without anti-OPN antibodies. The cell migrations were monitored for 24 hours. The migration of cells was determined by the number of cells that crossed into the wounded area from their reference point at time zero.

Colony Formation on Soft Agar

The 24-well plates were coated with 0.5 ml of 0.5% agar solution. MDA-MB-435s cells were suspended in 0.3% agar solution and plated

on top of the preset agar base and allowed to set. Every other day, 0.2 ml of medium with or without anti-OPN antibodies was refed to each well. After 10 days, photographs were taken. The colony formation ability was evaluated by counting the size of colonies containing more than 10 cells.

Human Umbilical Vein Endothelial Cell Proliferation Assay

The HUVECs were seeded at 2×10^4 cells per well in 96-well plates and allowed to adhere overnight before experimentation. They were serum-starved, and OPN with or without anti-OPN antibodies were added for 24 hours. Then 1-μCi per well ^{3}H-thymidine was added and incubated for an additional 6 hours at 37°C. Cells were washed, fixed with 10% trichloroacetic acid, and counted. All assays were performed in triplicates and repeated three times.

Human Umbilical Vein Endothelial Cell Apoptosis Assay

Apoptosis was induced in HUVECs by serum deprivation as previously described [12]. The apoptosis of HUVEC was demonstrated by nuclear fragmentation of 4′-6-diamidino-2-phenylindole (DAPI)–stained cells. To determine the apoptosis of HUVEC by FACScan analysis, HUVECs were seeded at a density of 2×10^5 cells per well in 6-well plates, and cultured in complete medium for 24 hours. The cells were then incubated for 24 hours of different treatments. The cells were stained with fluorescein isothiocyanate (FITC)–conjugated annexin V/propidium iodide (PI) and analyzed by flow cytometry. The extent of the apoptosis was quantified as a percentage of annexin V–positive cells.

Western Blot Analysis

Total protein was isolated from HUVECs receiving different treatments. SDS-PAGE (12%) gels were run and subsequently transferred to nitrocellulose membranes. The membranes were then blocked in 10% milk in PBS overnight at 4°C. Primary antibodies (Bcl-2, Bax, and β-actin) were added for 1 hour at room temperature followed by the appropriate HRP-conjugated secondary antibody at a dilution of 1:2000. Membranes were exposed to chemiluminescence reagents for 1 minute, and bands were detected by exposing to an x-ray film.

Electrophoretic Mobility Shift Assay

The DNA activity of nuclear factor κB (NF-κB) was determined by electrophoretic mobility shift assay (EMSA). A double-stranded oligonucleotide containing the DNA-binding site for the NF-κB proteins (forward, 5′ AGTTGAGGGGACTTTCCCAGGC 3′; reverse, 5′ GCCTGGGAAAGTCCCCTCAACT 3′) was end-labeled using biotin. The HUVECs were treated with OPN with or without anti-OPN antibodies for 6 hours. Nuclear proteins were extracted with NE-PER nuclear and cytoplasmic extraction reagents (Pierce, Rockford, IL). The nuclear extracts (3 μg) were incubated with 20 fmol of biotin-labeled double-stranded NF-κB oligonucleotide in binding buffer. The DNA-binding complex was resolved on a native polyacrylamide gel and was analyzed.

Capillary Tube Formation of HUVECs

Capillary tube formation by HUVECs was assayed on Matrigel. To prepare a gel, 100 μl of Matrigel thawed on ice overnight was added to each well of a 96-well microtiter plate. After polymerization of the gel, 2×10^4 HUVECs were plated onto the gel in Medium 200. In some wells, OPN with or without anti-OPN antibodies were added to the cells at the time of incubation. The capillary tube formation was observed under an inverted microscope.

Quantitative Determination of VEGF Expression in HUVEC

The HUVECs were treated with OPN with or without anti-OPN antibodies for 24 hours. Templates for real-time polymerase chain reaction (PCR) were obtained by reverse transcription reaction of total RNA. Primers for VEGF is as follows: forward, 5′-ATC ACG AAG TGG TGA AGT TC-3′; and reverse, 5′-TGC TGT AGG AAG CTC ATC TC-3′. Polymerase chain reaction cycling conditions were 95°C for 15 seconds and 60°C for 1 minute for 40 cycles. SYBR Green kit (Takara, Shiga, Japan) was used to quantify the PCR products. The *GAPDH* gene was used as an endogenous control to normalize for differences in the amount of total RNA in each sample.

Chicken Embryo Chorioallantoic Membrane Assay

Gelatin sponge was supplemented with 1) vehicle in PBS alone (negative control), 2) OPN (200 ng), 3) OPN and anti-OPN antibody (1 μg), or 4) VEGF (200 ng, positive control). The chorioallantoic membrane (CAM) of chicken eggs was added, on day 8, with 1-mm^3 sterilized gelatin sponges. At day 12, CAM was photographed *in ovo* with a stereomicroscope equipped with a digital camera. The angiogenesis response was evaluated as the number of vessels converging toward the gelatin sponge [18].

Rabbit Corneal Micropocket Assay

Slow-release pellets were prepared by mixing aliquots of OPN/sucralfate solution with or without anti-OPN antibodies (1 μg) and 12% Hydron stock solution. New Zealand white rabbits were anesthetized, and topical anesthesia was applied to the corneal surface. A 3-mm incision was made at the center of the cornea, and a micropocket was created in the cornea stroma, which extended 1 mm away from the limbus. The pellets were advanced into the corneal stromal pocket.

The corneas of the rabbits were examined in a masked manner by a slit lamp microscope at 10× magnification. The vascular response was measured as the maximal vessel length (VL) extending from the limbal vasculature toward the pellet and the contiguous circumferential zone of neovascularization (CN = clock hours of neovascularization, where 1 clock hour equals 30° of arc). The area of neovascular response was calculated using the formula: area (mm^2) = $0.2 \times \pi \times$ VL (mm) × CN (mm).

In Vivo *Xenograft Animal Study*

Female athymic mice (~4–6 weeks) were anesthetized and a small incision (0.5 mm) was made in the skin over the lateral thorax below the right limb. The mammary fat pads (MFPs) were exposed, and MDA-MB-435s cells (5×10^6 in 100 μl of Dulbecco's modified Eagle's medium) were orthotopically injected into the MFP. A minimum of 12 animals was used per group. Among them, six animals were used to observe primary tumor growth rate and terminated at 12 weeks, and six were used to determine spontaneous lung metastasis and terminated when primary tumor volume reached 1000 mm^3. For antibody treatment, the mice were treated twice per week with anti-OPN scFv-Fc (5 mg/kg body weight, intraperitoneally), and the control groups were treated with PBS and control scFv-Fc (7B6, 5 mg/kg body weight,

intraperitoneally). The treatment duration was 4 weeks. At the end of the experiment, mice were killed, and primary tumors and lungs were removed, fixed, and embedded.

Tumor and lung tissue sections were processed by hematoxylin and eosin staining for primary tumor and metastasis foci. For every two sections, the lung metastasis foci were counted. The grades of metastasis foci were determined as follows: grade 1, <20 cells/foci; grade 2, 20 < cells < 50/foci; grade 3, 50 < cells < 100 cells/foci; grade 4, >100 cells/foci. The total number of metastasis foci was counted as grade 1 × 1 + grade 2 × 2 + grade 3 × 3 + grade 4 × 4.

Anti-CD31 antibody was used to identify capillary-sized vessels in frozen sections of primary tumors. The tumor sections were incubated with rat antimouse CD31 overnight at 4°C. After being washed with PBS, the slides were incubated with goat antirat antibody conjugated to PE for 1 hour in the dark. The microvessel counting procedures as described by Weidner [19] was used. The microvessel density (MVD) was expressed as the number of vessels per square millimeter.

For immunofluorescence double staining of CD31/TUNEL, the sections were stained with CD31, and washed with PBS. TUNEL was performed using a commercial kit (Calbiochem, San Diego, CA). The sections were examined with under an Olympus Inverted System (Olympus, Tokyo, Japan).

Epitope Mappings

Epitope mappings of anti-OPN antibodies were performed using Ph.D.-7 Phage Display Peptide Library Kit (New England Biolabs, Inc., Ipswich, MA). After three rounds of panning, the phages eluted were then cloned and amplified for DNA sequencing and immunoanalysis.

Statistical Methods

Data were analyzed using the unpaired *t* test with 2-tailed *P* value or analysis of variance (for multiple comparisons) to calculate the statistical significance between control and treated groups. The results were presented as means ± SEM. Statistically significant differences were defined as having $P < .05$.

Results

Construction and Biopanning of Antihuman OPN Immunized Phage Library

Anti-OPN antibody library was constructed from human OPN-immunized mice (Figure 1*A*). The antibody library size was determined after serial dilution of the bacteria plated onto SOBAG plates (Gibco, Portland, OR), which was 5×10^8 colony-forming units. Four rounds of biopanning were performed to select specific anti-OPN antibodies. In total, 120 colonies were randomly picked out and tested by monoclonal ELISA after biopanning procedures, yielding 21 OPN-specific antibodies. Four unique anti-OPN phage scFvs were identified (1A12, 2H8, 7B6, and 7H12) by sequence analysis of the individual clones. The reactivity of anti-OPN antibodies to OPN is shown in Figure 1*B*.

The phage scFvs were cloned into the scFv-Fc expression cassette and expressed in Chinese hamster ovary cells as Fc fusion proteins. Recombinant scFv-Fc protein was batch-purified by Protein A column. SDS-PAGE analysis in denatured conditions revealed that the molecular weight of scFv-Fc was approximately 60 kDa. Western blot analysis confirmed that the purified scFv-Fc fusion protein specifically reacted with recombinant human OPN as the antigen (Figure 1*C*). To assess the specificity of purified scFv-Fc fusion proteins, competitive ELISA was performed to determine the binding specificity. As shown in Figure 1*D*, in the presence of the competitor (scFv-Fc), the phage scFv tested was partially inhibited from subsequent binding to the plated OPN antigen. The inhibition percent of phage scFv (10^{11} plaque-forming units/ml) was 40% when 10 μg/ml of scFv-Fc was added as the competitor.

Anti-OPN Antibodies Inhibited MDA-MB-435s Cell Attachment, Invasion, Migration, and Colony Formation in Soft Agar

To investigate the interaction of OPN with MDA-MB-435s cells, we performed cell attachment assay. As shown in Figure 2*A*, 1A12 and 2H8 blocked the cell attachment of MDA-MB-435s cells to human OPN, whereas 7B6 and 7H12 did not block the attachment of MDA-MB-435s cells on plates coated with 10 μg/ml of OPN. Because we found that anti-OPN antibody 7B6 did not inhibit cell attachment and invasion, we used 7B6 as the control antibody in the following experiments.

Matrigel invasion assay was used to determine whether anti-OPN antibodies had blocking functions toward the invasion. MDA-MB-435s cells were seeded on Matrigel inserts, and OPN was added in the lower chamber. After 24 hours of incubation, the cells on the lower surface of the filters were counted. 1A12 and 2H8 significantly inhibited cell invasion through Matrigel-coated filters compared with 7B6 and 7H12 [32 ± 4 *vs* 90.7 ± 7 (number of invaded cells ± SD)]. These results are shown in Figure 2*B*.

Cells exposed to anti-OPN antibodies were analyzed for their rate of migration. More cells appeared in the wounded gap, which represented enhanced healing of the wounded area. The cells crossed the line during 24 hours was taken as an index of wound healing. As shown in Figure 2*C*, the MDA-MB-435s cells treated with 1A12 and 2H8 migrated across an artificial *in vitro* wound much less efficiently than the control antibody.

We examined the efficacy of the anti-OPN antibodies in inhibiting breast cancer cell anchorage–independent growth (soft agar colony formation) *in vitro* because this activity correlates closely with tumorigenicity *in vivo* [20]. Anti-OPN antibodies significantly altered soft-agar colony-forming activity. As shown in Figure 2*D*, the clone sizes of 1A12- and 2H8-treated cells were significantly smaller than those of the control antibody-treated cells.

Anti-OPN Antibodies Inhibited OPN-Mediated Antiapoptotic and Prosurvival Functions

We investigated the effect of OPN on proliferation and apoptosis of HUVEC. The addition of OPN to the serum-deprived HUVECs reduced the amount of cell death. In the presence of OPN, ^{3}H-thymidine uptake increased 3.08 ± 0.64-fold in HUVECs (Figure 3*A*, $P < .01$); however, this incorporation uptake decreased 2.76 ± 0.35-fold when anti-OPN antibodies were added. Our results showed that OPN may support cell survival under conditions of serum withdrawal, conditions that have been shown to induce HUVEC apoptosis. In the presence of anti-OPN antibodies, the prosurvival function of OPN was inhibited significantly.

Induction of apoptosis was analyzed with the help of DAPI, which caused a regular staining in intact nuclei, but an irregular staining in apoptotic cells [21]. As shown in Figure 3*B*, ~30% of HUVECs lost membrane integrity after treatment with serum deprivation for

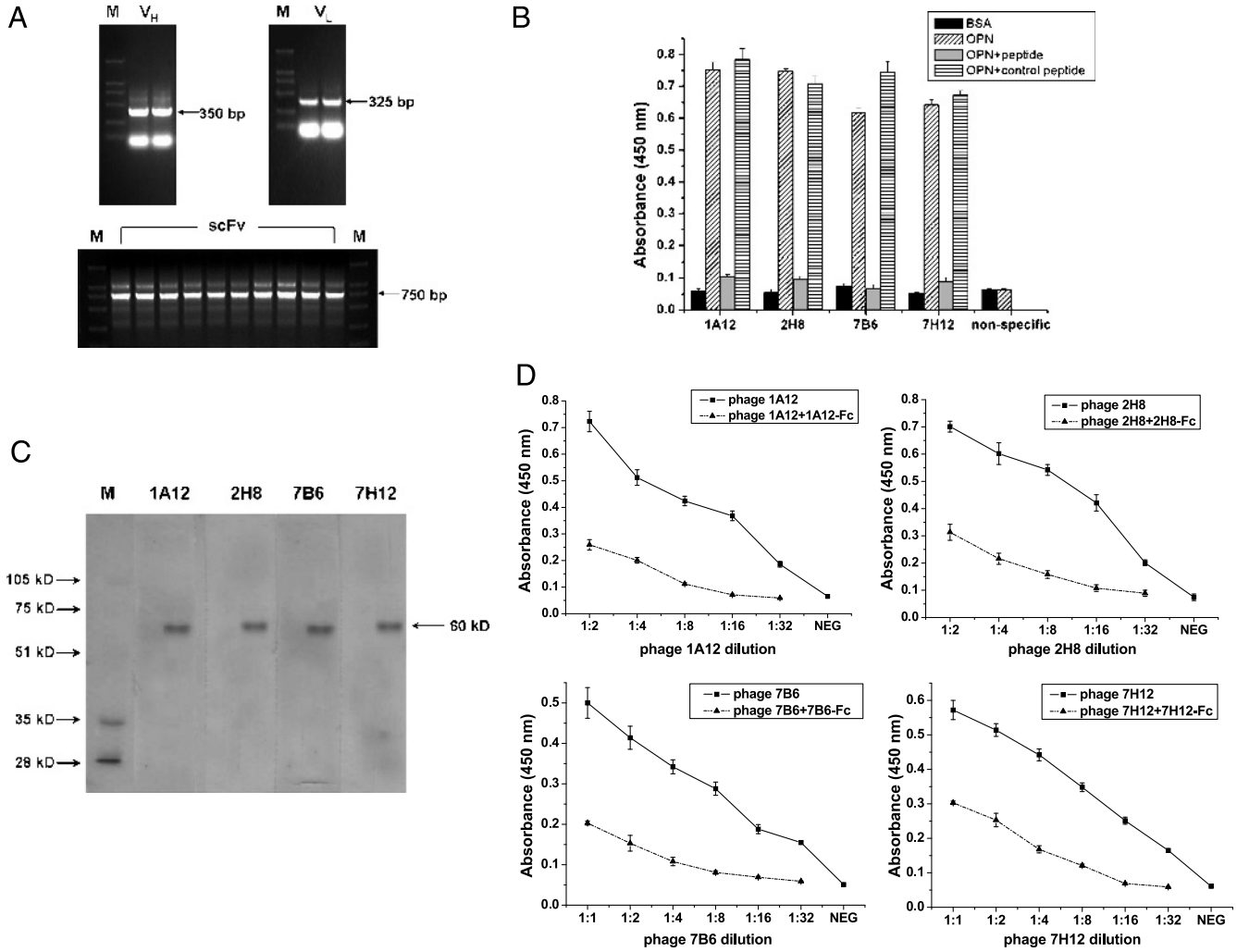

Figure 1. The construction and biopanning of phage antibody library. (A) Construction of phage antibody library. Electrophoresis was performed on 1% agarose gel, and PCR products were visualized by ethidium bromide. The lengths of V_H, V_L, and scFv were approximately 350, 325, and 750 bp, respectively. (B) Binding of positive clones to immobilized OPN. After immobilization of OPN on 96-well microtiter plates, wells were washed and incubated with different phage scFv clones. Unbound phage scFvs were washed away, and bound phage scFvs were detected by HRP-conjugated anti-M13 antibody. BSA was used as negative control antigen. (C) Western blot analysis of scFv-Fc. *Lane M* indicates marker protein; 1A12, 2H8, 7B6, 7H12, different scFv-Fc. The results confirmed that the purified scFv-Fc fusion protein specifically reacted with recombinant human OPN as the antigen. The band was approximately 60 kDa. (D) Competitive ELISA was performed to determine the competitive binding inhibition between phage scFv and scFv-Fc. Inhibition of phage scFv binding to OPN was observed by using scFv-Fc fusion protein as a competitor. The bound phages were detected by ELISA with HRP-conjugated anti-M13 antibody. Comparable data were obtained in three independent experiments.

24 hours, compared with ~10% of cells in control cultures treated with the normal serum culture condition. The HUVECs treated with OPN showed less DAPI-stained cells compared with nontreated ones. The addition of anti-OPN antibodies abrogated the function of OPN.

FACScan analysis of annexin V/FITC-PI staining showed that serum deprivation induced apoptosis of HUVECs. Exogenous soluble OPN protected HUVECs from serum deprivation–induced apoptosis. Anti-OPN antibodies inhibited OPN-mediated antiapoptotic function on HUVECs (Figure 3*C*).

The expressions of apoptosis-related proteins (Bcl-2 and Bax) were analyzed by Western blot analysis. The HUVECs were deprived of factors as described above, with or without OPN and anti-OPN antibodies. Proapoptotic Bax expression was upregulated when anti-OPN antibodies were added compared with OPN alone. Conversely, antiapoptotic Bcl-2 expression was downregulated (Figure 3*D*).

The nuclear extracts were prepared and used for EMSA using biotin-labeled NF-κB oligonucleotides. The results are shown in Figure 3*E*. In OPN-treated HUVECs, the NF-κB pathway was activated, which provided a protective function to the cells. The DNA-protein complex was specific, as unlabeled NF-κB oligomer inhibited the signal, whereas unrelated oligomer had no effect. In contrast, cells pretreated with anti-OPN antibodies did not induce NF-κB activity, and the control antibody had no effect inhibiting protective function of OPN.

Anti-OPN Antibodies Interfered with Angiogenesis In Vitro *and* In Vivo

The effect of anti-OPN antibodies on capillary tube formation of the HUVECs on the Matrigel was evaluated. Osteopontin-cultured

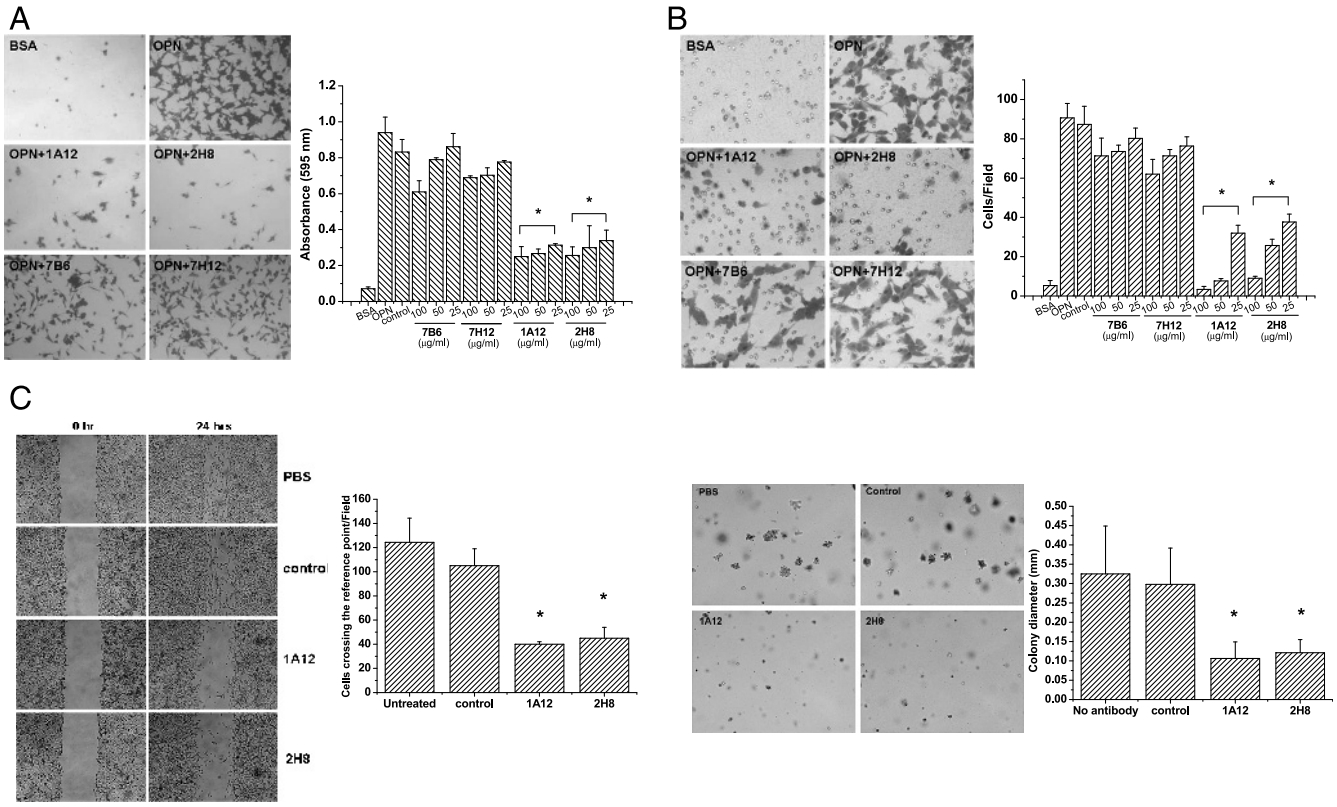

Figure 2. *In vitro* function of anti-OPN antibodies. (A) Cell attachment of MDA-MB-435s cells was inhibited by anti-OPN antibodies. MDA-MB-435s cells were plated on wells coated with 10 μg/ml of OPN in plating medium alone or medium containing anti-OPN antibodies. 1A12 and 2H8 inhibited cell attachment to OPN at the concentration of 25 μg/ml. 7B6 and 7H12 did not have this effect. The inhibition rate of 1A12 and 2H8 (25 μg/ml) was approximately 60%. *$P < .05$. (B) Anti-OPN antibodies inhibited Transwell invasion of MDA-MB-435s cells. MDA-MB-435s cells in plating medium alone or in plating medium containing anti-OPN antibodies were seeded on polycarbonate filters with OPN in the lower chamber of Transwell system. Cells that invaded through the filter in response to OPN in the lower chamber were quantified by cell staining. The error bars represent the SD from three independent experiments. 1A12 and 2H8 (25 μg/ml) significantly inhibited cell invasion, whereas 7B6 and 7H12 did not have an inhibitory effect. *$P < .05$. (C) Scratch wound healing assay. MDA-MB-435s cells were grown in monolayer until confluent and were then serum-starved. After being wounded, the monolayers were treated with anti-OPN antibodies for 24 hours. 1A12 and 2H8 (25 μg/ml) inhibited MDA-MB-435s cell migration. The graph showed the mean and SD of values from a representative experiment performed in triplicate. The results were similar in repetitions. *$P < .05$. (D) Anti-OPN antibodies inhibited MDA-MB-435s colony formation in soft agar. The clone sizes of the anti-OPN antibody group (1A12 and 2H8) were smaller than the clone sizes of the untreated and control groups. *$P < .05$.

HUVECs developed tube formation and complete networks within 12 hours. The HUVECs incubated with OPN plus anti-OPN antibodies did not form complete capillary-like structures. In the presence of the control antibody (7B6), tube formation was not inhibited. Representative pictures are shown in Figure 4*A*. Tube length per field was calculated at time point of 4, 6, and 8 hours after treatment. The results of this *in vitro* assay indicated that anti-OPN antibodies had potential antiangiogenic activity.

Quantitative reverse transcription–PCR showed that treatment with OPN increased the mRNA expression of VEGF compared with untreated HUVECs. When HUVECs were pretreated with anti-OPN antibodies and OPN was added, there was not an increase in VEGF mRNA expression level (Figure 4*B*).

The effects of anti-OPN antibodies on blood vessel formation were monitored on the CAM of 8-day-old chicken embryos. As shown in Figure 4*C*, OPN induced a strong angiogenic response in the CAM, similar to that of VEGF. No vascular reaction was detectable in the embryos treated with PBS. Anti-OPN antibodies showed a strong and reproducible antiangiogenic effect in the CAM assay. Few blood vessels penetrated into the region where the anti-OPN antibodies were applied. In contrast, the control antibody did not have this effect.

To further investigate the function of anti-OPN antibodies on angiogenic activity *in vivo*, OPN-induced rabbit corneal neovascularization was studied. On the seventh postoperative day, the rabbits showed no signs of discomfort. Slit lamp observation reveled that all eyes were noninflammatory, and no edema was observed in any of the eyes. Control pellets with only PBS did not induce an angiogenic response. Implants containing VEGF and OPN induced corneal neovascularization. In the presence of 1A12 and 2H8, angiogenesis toward OPN was significantly inhibited. Implants containing OPN plus control antibody still gave positive response. The vascular areas of anti-OPN antibody groups were decreased by 60% ($P < .01$; Figure 4*D*) compared with control. Representative corneas were examined histologically and no neutrophils were found, indicating that nonspecific inflammation was not a contributing factor in any of the corneal responses (data not shown). These findings demonstrated that anti-OPN antibodies had inhibitory function toward angiogenesis *in vivo*.

Tumor Growth and Spontaneous Lung Metastasis of MDA-MB-435s Cells in Nude Mice Were Inhibited by Anti-OPN Antibodies

Because expression of OPN by breast cancer cells contributes to tumor growth and metastasis, we next determined the effect of anti-OPN antibodies on breast cancer xenograft model. MDA-MB-435s cells were xenografted into the MFP of female nude mice to observe tumor growth and spontaneous lung metastatic ability. Primary tumors became readily apparent approximately 2 weeks after injection and tumor take was 100%. 1A12 and 2H8 group had a longer latency period, taking approximately 8 weeks to reach a mean tumor volume of ~100 mm^3 compared with PBS and control antibody group approximately 4 weeks. Tumors treated by 1A12 were also less vascularized, especially in the periphery where angiogenesis was prominent. Overall, tumors from the PBS and control antibody groups grew at a more accelerated rate than those of the 1A12 and 2H8 groups, producing significantly larger tumor volumes from week 2 to 12 ($P < .01$; Figure 5*A*).

The lung metastasis foci were examined under a microscope. Representative histological sections of spontaneous lung metastases are shown in Figure 5*B*. The incidence of spontaneous lung metastasis was significantly higher in PBS and control groups. Whereas only 16.7% (1 of 6 from the 1A12- and 2H8-treated groups) of mice had metastasis foci in the lungs, 83.3% (5 of 6) of the mice in the PBS and control groups had multiple metastasis foci in the lungs. The metastasis foci were observed on the lung surface and as clusters in interior regions. In the PBS-treated mice, the metastasis foci contained much larger, densely packed tumor masses, sometimes the tumor masses merged to bigger clusters, whereas the anti-OPN antibody-treated mice had much smaller metastasis foci. We also compared the different grades of lung metastasis foci. The grades of metastasis foci were mainly grades 2 to 3. These results show that, in this spontaneous metastasis model, anti-OPN antibodies were highly effective in reducing lung metastasis.

We determined whether blockade of OPN by antibodies could result in the suppression of tumor angiogenesis. Tumor-associated

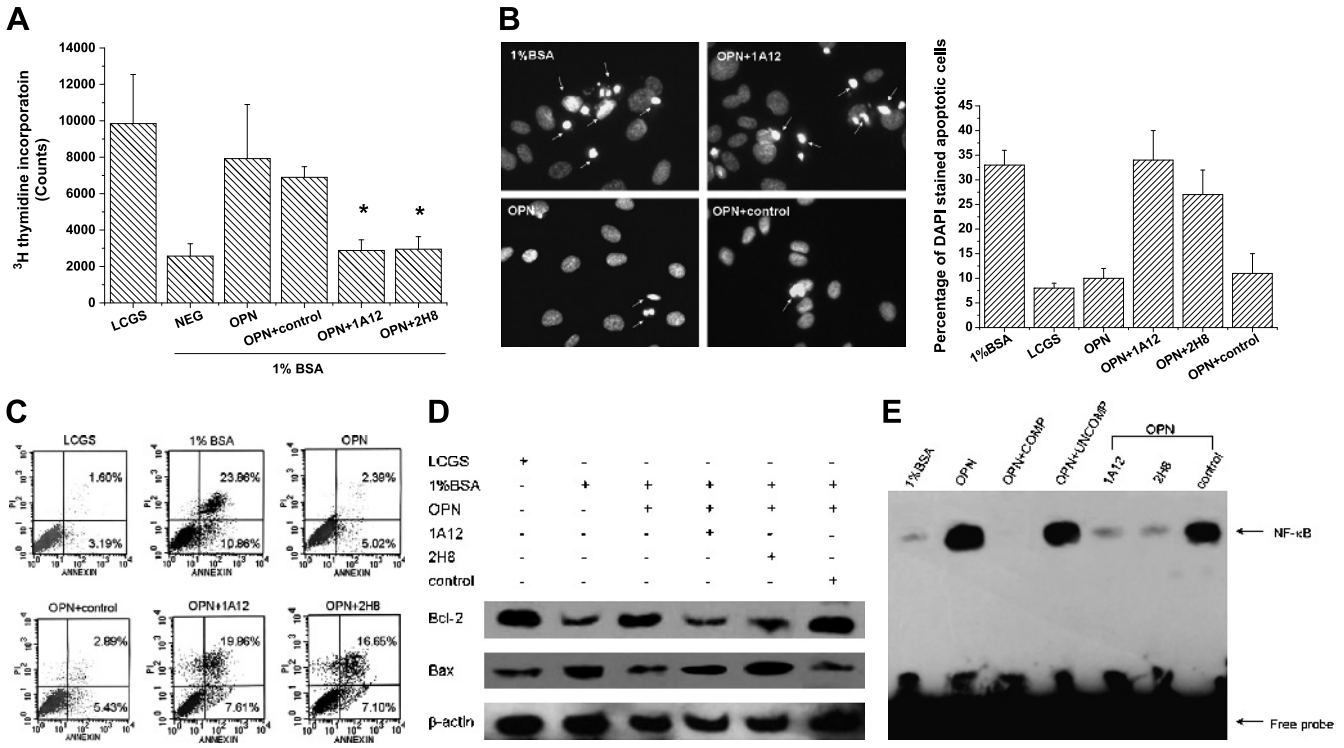

Figure 3. Effect of anti-OPN antibodies on serum deprivation–induced apoptosis in HUVECs. (A) ^{3}H-thymidine incorporation uptake in HUVECs. The HUVECs were maintained in Medium 200 supplemented with low serum growth supplement and were incubated for 24 hours. Then the cells were extensively washed with PBS, and the medium was changed to serum-free Medium 200 containing OPN with or without anti-OPN antibodies and incubated for 24 hours. Cell proliferation was assayed 24 hours after serum deprivation. ^{3}H-thymidine incorporation uptake was examined to present DNA synthesis. Data were expressed as mean ± SD of three experiments. *$P < .05$. (B) DAPI staining of apoptotic cells. Nuclear morphology was examined by DAPI staining as described in the Materials and Methods section. Note the nuclear condensation and fragmentation in the serum deprivation group, which was indicative of apoptosis. (C) The apoptosis of HUVECs was determined by annexin V/PI staining and FACScan analysis. The percentage of cells found in each quadrant of the dot plot is depicted. Results are shown as representative of three independent experiments. Placement of HUVEC in the minimal medium for 24 hours significantly induced apoptosis when compared with the untreated cells. Treatment of HUVEC in the minimal medium with OPN resulted in a significant decrease in the number of apoptotic cells. Data shown were the means of three separate experiments ± SD ($P < .01$, 1% BSA *vs* untreated). Anti-OPN antibodies 1A12 and 2H8 abrogated the antiapoptotic function of OPN. (D) Bcl-2 family proteins were analyzed by Western blot analysis. The HUVECs were cultured in the presence or absence of OPN (with or without anti-OPN antibodies) for 24 hours. After cultivation, we assessed the expression of Bcl-2 and Bax in HUVECs using Western blot analysis as described in the text. (E) Electrophoretic mobility shift assay was performed to determine the NF-κB activity of OPN- and anti-OPN antibody–treated HUVECs. Compared with untreated HUVECs, OPN treatment activated NF-κB activity, and anti-OPN antibody treatment abrogated this function.

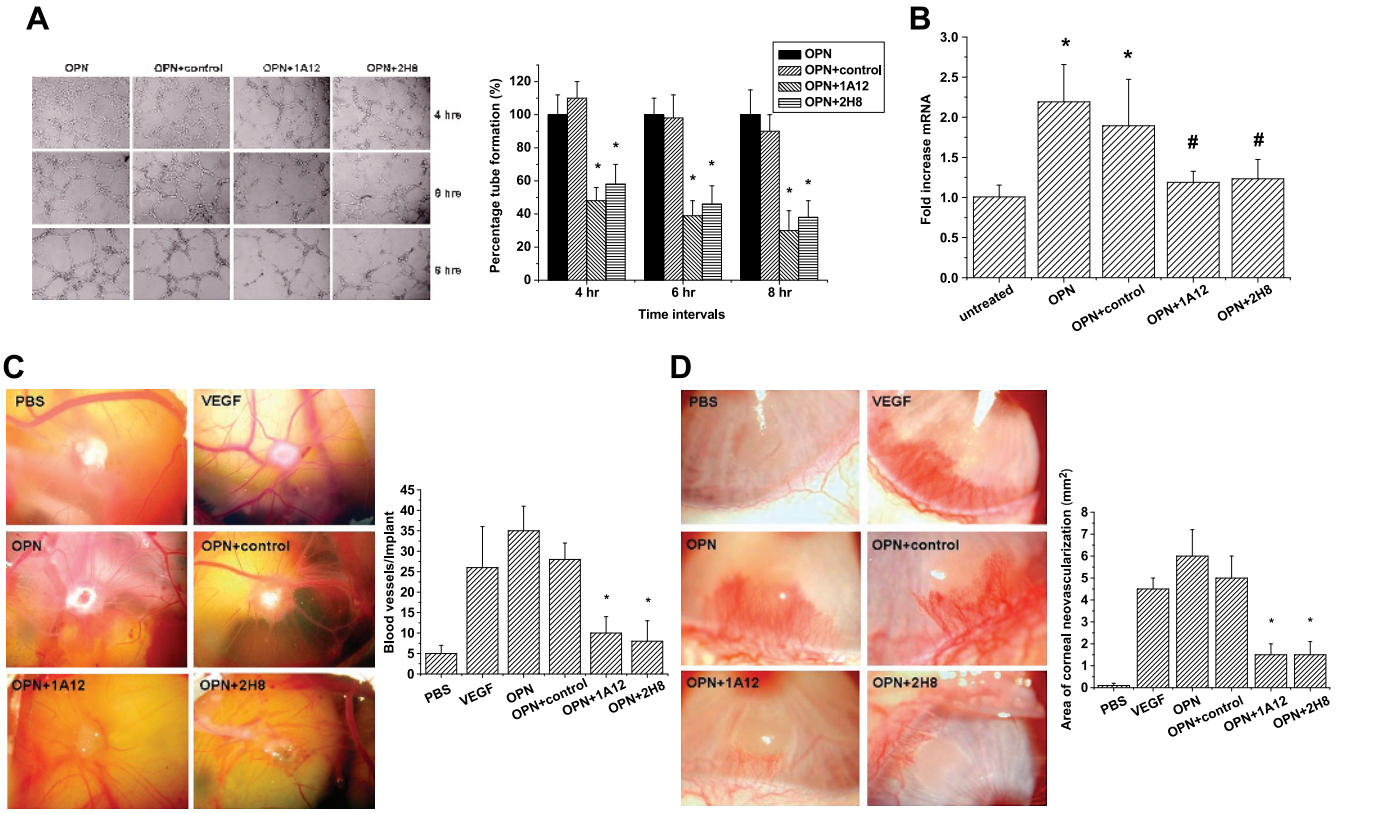

Figure 4. Antiangiogenesis effect of anti-OPN antibodies. (A) Inhibitory effect of anti-OPN antibodies on *in vitro* HUVEC capillary tube formation. The HUVECs were plated on Matrigel (100 μl per well) at a density of 1×10^4 cells per well and treated with OPN in the absence and presence of anti-OPN antibodies. The ability to form tubes was inhibited in the presence of anti-OPN antibodies. The experiment was repeated three times, and representative pictures are shown. *$P < .05$. (B) Quantitative real-time PCR determination of VEGF mRNA expression. Vascular endothelial growth factor mRNA expression was determined after treatment of HUVEC with OPN with or without anti-OPN antibodies. There was an increase in VEGF mRNA expression treated with OPN compared with that of untreated group. When anti-OPN antibodies were added together with OPN, this increase was not observed. *$P < .05$. (C) Chicken embryo CAM assay. Osteopontin was angiogenic in the chicken embryo CAM assay. On day 8, gelatin sponges loaded with OPN (200 ng), VEGF (200 ng), or PBS was applied to the chicken CAM, and its effect on vascular development was evaluated. In some experiments, 1 μg of 1A12 and 2H8 was added simultaneously with OPN to examine its ability to inhibit the OPN-induced angiogenic response. Neovascularization was observed in OPN and VEGF group, whereas no vascular response was observed in control CAM with PBS. In the presence of 1A12 and 2H8, the angiogenesis responses were significantly reduced. Experiments were repeated three times, with a minimum of eight embryos in each treatment group. *$P < .05$. (D) Anti-OPN antibodies inhibited angiogenesis mediated by OPN in the rabbit corneal micropocket assay. Representative slit lamp photographs of rabbit corneas on day 7 after implantation with Hydron/sucralfate pellets containing 1) OPN alone (200 ng), 2) OPN and anti-OPN antibodies, 3) OPN and control (7B6), 4) PBS, and 5) VEGF (200 ng). The results showed that OPN alone induced a neovascular response from the limbal vessels and reached toward the pellet. Anti-OPN antibodies inhibited the neovascular response when added together with OPN. No response was observed when PBS pellet was implanted. *$P < .05$.

neovascularization as indicated by MVD was examined by immunohistochemistry using anti-CD31 antibody. As shown in Figure 5*C*, we found a significant reduction in tumor MVD/field after treatment with anti-OPN antibodies compared with those of PBS and control antibody groups. These results suggest that the inhibition of tumor growth by anti-OPN antibodies is partly caused by the suppression of tumor angiogenesis.

We also determined whether anti-OPN antibodies inhibited the function or induced apoptosis of tumor endothelial cells. CD31 (*red*)/TUNEL (*green*) double labeling revealed that endothelial cells were only in the tumors of mice treated with anti-OPN antibodies. Apoptotic endothelial cells were not identified in the tumor of PBS- or control-treated mice (Figure 5*D*).

Mapping of Epitopes

Sequence analysis of peptides reactive to anti-OPN antibodies showed that the epitope of 1A12 was located within the C-terminal amino acids of human OPN (Asn-Ala-Pro-Ser-Ser-Asp, amino acids 212-216), and the epitope of 2H8 was targeted to a classic epitope Gly-Arg-Gly-Asp-Ser, as shown in Table 1. The epitope of 7B6 was located within the exon 4 of human OPN. Researches have shown that the OPN molecule contains multiple binding sites in addition to the classic arginine-glycine–aspartic acid sequence. These epitopes of the OPN molecule interact with different cellular receptors and modulate distinct cellular functions [22]. The different epitopes of the anti-OPN antibodies might help explain the different functions of the antibodies.

Discussion

Osteopontin plays an important role in the steps toward cancer cell metastasis, including binding to cell receptors and communicating the signals that determine cell proliferation, migration, and invasion.

Transformed cells are often characterized by the abundant secretion of OPN [23], including breast cancer, prostate cancer, osteosarcoma, and squamous cell carcinoma. Breast cancer cells themselves are capable of secreting OPN, which shows promise as a prognostic marker in breast cancer patients [24]. MDA-MB-435s cell line, which expresses and secretes OPN, is known to be tumorigenic and highly metastatic, and it was used in the xenograft tumor model in our study.

To inhibit the function of OPN, we used phage antibody display technology and successfully generated a panel of OPN-specific scFvs using phage antibody library. After sequence analysis, we chose four of them to study their function *in vitro* and *in vivo*. The fusion to Fc fragment gave scFv prolonged serum half-life and provided a simple route for purification through Protein A affinity chromatography.

Detachment and migration from the primary tumor and invasion of surrounding blood or lymphatic vessels are critical and complex steps in clinically metastatic diseases. We used scratch wound healing assay to determine the efficacy of anti-OPN antibodies in inhibiting tumor cell migration. Matrigel invasion assay was used to determine the ability of tumor cells to cross the basement membrane. In *in vitro* studies of cell attachment, migration, and invasion, anti-OPN antibodies 1A12 and 2H8 successfully inhibited these functions, which simulated the *in vivo* conditions of animals. The capacity of cells to grow in semisolid medium is supposed to reflect the cells' independence of contact with a physiologically relevant extracellular matrix. When anti-OPN antibodies 1A12 and 2H8 were added in the soft agar, the anchorage-independent growth was significantly inhibited. We proposed that the antibodies might neutralize the OPN secreted by the tumor cells and interrupt the ligation of OPN to its receptors.

We investigated the ability of OPN to protect HUVECs against serum deprivation–induced apoptosis, and this function can be significantly inhibited by the pretreatment of anti-OPN antibodies.

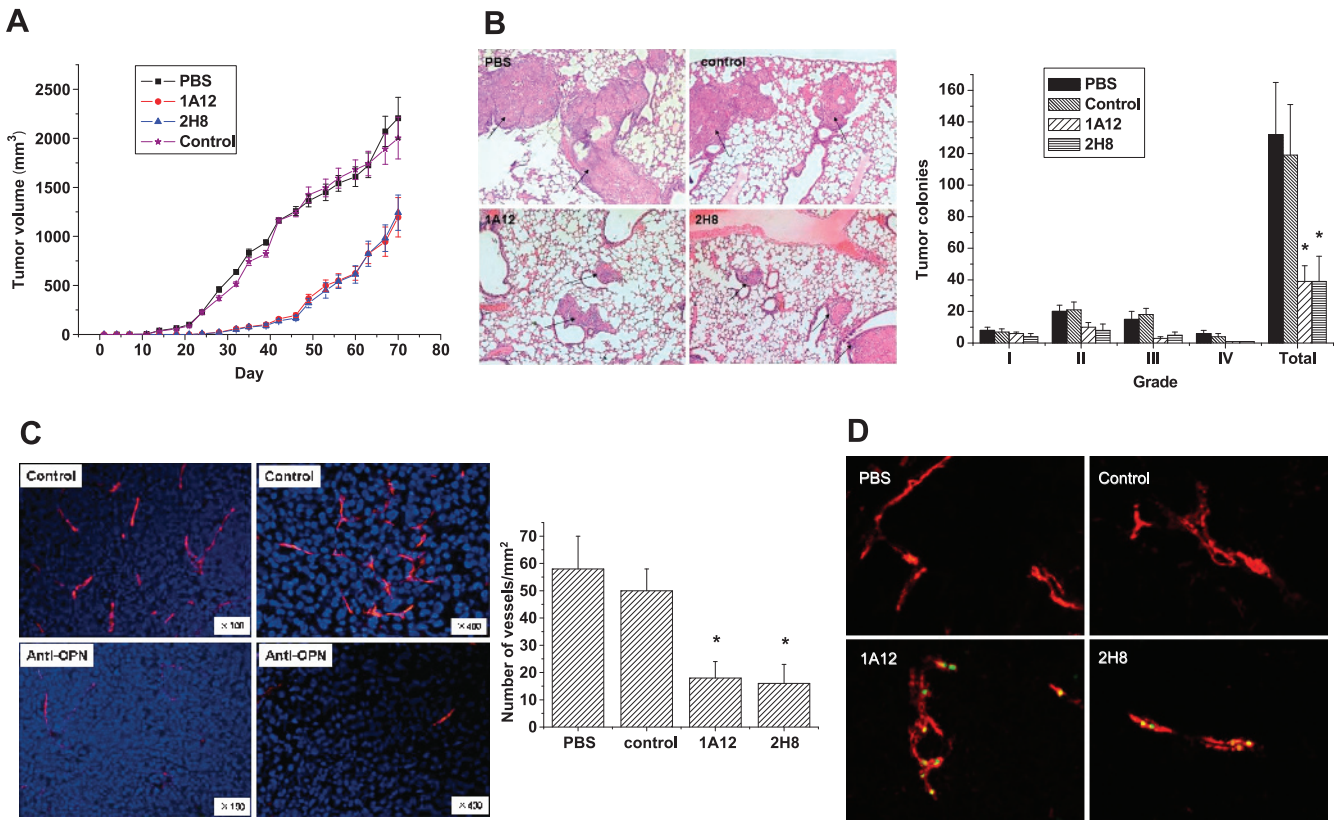

Figure 5. *In vivo* study of anti-OPN antibodies. (A) Efficacy of anti-OPN antibodies on the primary tumor volume of MDA-MB-435s cells orthotopic xenografts in nude mice. Animals were divided into four experimental groups receiving different treatments. Anti-OPN antibodies (1A12, 2H8, and 7B6) or PBS was administrated at 5-mg/kg body weight twice per week beginning at the time of tumor cell implantation in the MFP. The experiment was terminated after 12 weeks of initial inoculation. The tumors were measured twice per week with calipers, and tumor volumes were calculated. (B) Lung metastasis of breast cancer xenograft model. Female nude mice were given injections of 5×10^6 MDA-MB-435s cells into the MFP. Representative lung tissue sections of hematoxylin and eosin staining from the nude mice after MFP injection of MDA-MB-435s cells with or without anti-OPN antibody treatment. *Arrows* indicate tumor metastasis sites. Anti-OPN antibodies treatment inhibited lung metastasis in the orthotopic model. The metastasis foci and grade decreased compared with those of the PBS and control groups. *$P < .05$. (C) Angiogenesis in tumor tissue sections after immunofluorescence staining of blood vessels with anti-CD31 antibody and MVD counting. Representative microscopic fields from the tumors showed a higher density of blood vessels in the PBS or control group than in the anti-OPN antibody groups. CD31-positive microvessels were stained in red and nuclei were stained by Hoechst 33258 in blue. Blood vessels in tumor sections stained with anti-CD31 were counted from five microscopic fields for all tumors from the six mice in each treatment group are shown. Results are the mean ± SD of six animals per group. *$P < .05$. (D) CD31/TUNEL double staining showed that no apoptotic endothelial cells appeared in the PBS or the control group, whereas in the tumors from anti-OPN antibodies groups, endothelial cells that underwent apoptosis were identified.

Table 1. Epitope Mappings of Anti-OPN Antibodies.

ScFv	Peptide Sequences	Possible Epitope	Location on Human OPN
1A12	DTENNNNGPSDX NAVNTNNAPTDY NALNHNNARSDY TTNPNNAPSSYA	NAPSD	AA 212-216
2H8	ANNGRGTNSXNN NPATSRNNDSNT TNTPGRVNSNNX YNGTGDATPNTY	GRGDS	AA 158-162
7B6 (control)	GTSTEVWLAPDP DVYWLMPDPPTS ATWLNPDPSQKQ TDTPWKFPDPSL	WLNPDP	AA 53-58

Sequence alignment of the possible epitope and the location of the possible epitope on human OPN sequence are shown. The epitope of 1A12 is located at amino acids 212 to 216 of human OPN, whereas the epitope of 2H8 is a classic one, GRGDS, which was reported as a cell-binding domain of OPN and other proteins. 7B6 was used as a control antibody, and its epitope was mapped to amino acids 53 to 58 of human OPN.
Identical amino acids are highlighted in the table.

DAPI staining of nuclear morphology of HUVEC confirmed serum deprivation in the induction of apoptosis. By ^{3}H-thymidine incorporation assay, we demonstrated that OPN was able to protect the survival of HUVECs under apoptotic condition. When anti-OPN antibodies–pretreated HUVECs were added with exogenous OPN, the cells could not be protected by OPN. FACScan analysis of annexin V/FITC-PI staining of apoptotic cells demonstrated the antiapoptotic function of OPN, and 1A12 and 2H8 inhibited the function of OPN. Western blot analysis showed that the antiapoptosis protein Bcl-2 was upregulated when treated with OPN, and compared with untreated HUVEC, the proapoptotic protein Bax was downregulated when treated with OPN. When anti-OPN antibodies were added, the functions of OPN were abrogated. The results of EMSA suggested that NF-κB was activated when OPN was added, and anti-OPN antibodies inactivated the function. These results were consistent with previous reports of antiapoptotic and prosurvival functions of OPN [12]. Endothelial cell and tumor cell interacted with each other to facilitate the invasion and migration of tumor cells [25]. Therefore, the antiapoptotic function of OPN might help to explain the metastasis ability of tumor cells that express OPN. Treatment with anti-OPN antibodies inhibited the antiapoptotic function of OPN and thus could help to inhibit tumor cell metastasis from blood vessel.

Angiogenesis plays a key role in many physiological processes and pathological processes such as the development and progression of tumors [26]. Tumor-associated neovascularization is necessary for the development and metastasis of solid tumors [27]. *OPN* is one of the genes differentially expressed during *in vitro* angiogenesis [28], and its expression has been correlated to VEGF expression [11,29], one of the most potent stimulator of angiogenesis. We studied anti-OPN antibodies in inhibiting angiogenesis *in vitro* and *in vivo*. The HUVEC capillary tube formation is a multistep process involving cell adhesion, migration, differentiation, and growth. Blockage of the function of OPN by anti-OPN antibodies interrupted the capillary tube formation process. Next, we determined the function of anti-OPN antibodies in *in vivo* models of angiogenesis. In agreement with the *in vitro* findings, OPN caused newly formed blood vessels of the chick embryo CAM. In the presence of the anti-OPN antibodies 1A12 and 2H8, this angiogenic effect of OPN was significantly inhibited. Rabbit corneal micropocket assay indicated that anti-OPN antibodies specifically suppressed OPN-induced corneal neovascularization *in vivo*. We performed the two *in vivo* angiogenesis assays to demonstrate that OPN may initiate the formation of new blood vessels, an event essential for tumor progression, and anti-OPN antibodies effectively inhibited the function of OPN in angiogenesis.

The metastatic disease requires that tumor cells complete all steps of a complex process. The formation of a secondary tumor colony in a distant organ is the culmination of a series of sequential and highly selective events [30]. We observed in a highly aggressive MDA-MB-435s xenograft animal model that primary tumor growth and spontaneous lung metastasis rate were significantly decreased in the presence of the anti-OPN antibodies 1A12 and 2H8, suggesting that these antibodies had inhibitory functions toward the function of OPN *in vivo*. Microvessel density in anti-OPN antibodies–treated tumors decreased significantly compared with those of the PBS or the control group, indicating that anti-OPN antibodies can block the angiogenic function of OPN *in vivo*. Reduced angiogenesis and increased endothelial cell apoptosis in these tumors are presumably contributing to the inhibition of tumor growth and spontaneous lung metastasis.

One of the major mechanisms by which OPN influences cell behavior is through interactions with various integrins, including $\alpha_v\beta_3$, $\alpha_9\beta_1$, $\alpha_v\beta_5$, and $\alpha_5\beta_1$. Osteopontin has multiple domains, and multiple forms of human OPN are generated by alternative splicing. Osteopontin has the arginine-glycine–aspartic acid domain for binding with integrins [31,32]. It also has a heparin-binding domain close to the carboxyl-terminus of the OPN protein involved in the binding to different isoforms of CD44 [33]. Furthermore, OPN contains the binding domain for calcium ions close to the carboxyl-terminus of OPN, and binding to calcium has been indicated to regulate interactions with integrin-binding domains [31]. Recent progress has defined that splice variant OPN-c is a highly specific marker for transformed cells [34]. In our study, the epitopes of 7B6 were mapped to the exon 4 of full-length human OPN (OPN-a), which is absent in the splice variant OPN-c. Because OPN-c strongly supported anchorage-independent growth, we deduce that only targeting OPN-a, but not OPN-c, was not sufficient to block the function of this diverse protein. We have found a new possible functional epitope near the calcium-binding loop of OPN, although the detailed function of the epitope still needs to be further investigated. A better understanding of the function/structure relationships will help clarify the different epitopes of OPN in various diseases.

In summary, the present study has provided four OPN-specific antibodies, and two of them are shown to possess inhibitory effects toward the functions of OPN *in vitro* and *in vivo*. On the basis of these observations, we speculate that these two anti-OPN antibodies have the potential for future therapeutic use.

References

[1] Kreunin P, Urquidi V, Lubman DM, and Goodison S (2004). Identification of metastasis-associated proteins in a human tumor metastasis model using the mass-mapping technique. *Proteomics* **4**, 2754–2765.
[2] Denhardt DT and Guo X (1993). Osteopontin: a protein with diverse functions. *FASEB J* **7**, 1475–1482.
[3] Weber GF (2001). The metastasis gene osteopontin: a candidate target for cancer therapy. *Biochim Biophys Acta* **1552**, 61–85.
[4] Rittling SR and Chambers AF (2004). Role of osteopontin in tumour progression. *Br J Cancer* **90**, 1877–1881.
[5] Tuck AB, Elliott BE, Hota C, Tremblay E, and Chambers AF (2000). Osteopontin-induced, integrin-dependent migration of human mammary epithelial cells involves activation of the hepatocyte growth factor receptor (Met). *J Cell Biochem* **78**, 465–475.

[6] Wong NC, Mueller BM, Barbas CF, Ruminski P, Quaranta V, Lin EC, and Smith JW (1998). alphav Integrins mediate adhesion and migration of breast carcinoma cell lines. *Clin Exp Metastasis* **16**, 50–61.

[7] Leali D, Dell'Era P, Stabile H, Sennino B, Chambers AF, Naldini A, Sozzani S, Nico B, Ribatti D, and Presta M (2003). Osteopontin (Eta-1) and fibroblast growth factor-2 cross-talk in angiogenesis. *J Immunol* **171**, 1085–1093.

[8] Liaw L, Lindner V, Schwartz SM, Chambers AF, and Giachelli CM (1995). Osteopontin and beta 3 integrin are coordinately expressed in regenerating endothelium *in vivo* and stimulate Arg-Gly-Asp–dependent endothelial migration *in vitro*. *Circ Res* **77**, 665–672.

[9] Scatena M, Almeida M, Chaisson ML, Fausto N, Nicosia RF, and Giachelli CM (1998). NF-kappaB mediates alphavbeta3 integrin-induced endothelial cell survival. *J Cell Biol* **141**, 1083–1093.

[10] Shijubo N, Uede T, Kon S, Nagata M, and Abe S (2000). Vascular endothelial growth factor and osteopontin in tumor biology. *Crit Rev Oncog* **11**, 135–146.

[11] Senger DR, Ledbetter SR, Claffey KP, Papadopoulos-Sergiou A, Peruzzi CA, and Detmar M (1996). Stimulation of endothelial cell migration by vascular permeability factor/vascular endothelial growth factor through cooperative mechanisms involving the alphavbeta3 integrin, osteopontin, and thrombin. *Am J Pathol* **149**, 293–305.

[12] Khan SA, Lopez-Chua CA, Zhang J, Fisher LW, Sorensen ES, and Denhardt DT (2002). Soluble osteopontin inhibits apoptosis of adherent endothelial cells deprived of growth factors. *J Cell Biochem* **85**, 728–736.

[13] Fedarko NS, Fohr B, Robey PG, Young MF, and Fisher LW (2000). Factor H binding to bone sialoprotein and osteopontin enables tumor cell evasion of complement-mediated attack. *J Biol Chem* **275**, 16666–16672.

[14] Oates AJ, Barraclough R, and Rudland PS (1996). The identification of osteopontin as a metastasis-related gene product in a rodent mammary tumour model. *Oncogene* **13**, 97–104.

[15] Denhardt DT and Chambers AF (1994). Overcoming obstacles to metastasis-defenses against host defenses: osteopontin (OPN) as a shield against attack by cytotoxic host cells. *J Cell Biochem* **56**, 48–51.

[16] Wu Y, Denhardt DT, and Rittling SR (2000). Osteopontin is required for full expression of the transformed phenotype by the *ras* oncogene. *Br J Cancer* **83**, 156–163.

[17] Wai PY, Mi Z, Guo H, Sarraf-Yazdi S, Gao C, Wei J, Marroquin CE, Clary B, and Kuo PC (2005). Osteopontin silencing by small interfering RNA suppresses *in vitro* and *in vivo* CT26 murine colon adenocarcinoma metastasis. *Carcinogenesis* **26**, 741–751.

[18] Barnhill RL and Ryan TJ (1983). Biochemical modulation of angiogenesis in the chorioallantoic membrane of the chick embryo. *J Invest Dermatol* **81**, 485–488.

[19] Weidner N (1995). Current pathologic methods for measuring intratumoral microvessel density within breast carcinoma and other solid tumors. *Breast Cancer Res Treat* **36**, 169–180.

[20] Janik P, Briand P, and Hartmann NR (1975). The effect of estrone-progesterone treatment on cell proliferation kinetics of hormone-dependent GR mouse mammary tumors. *Cancer Res* **35**, 3698–3704.

[21] Telford WG, King LE, and Fraker PJ (1992). Comparative evaluation of several DNA binding dyes in the detection of apoptosis-associated chromatin degradation by flow cytometry. *Cytometry* **13**, 137–143.

[22] Katagiri YU, Sleeman J, Fujii H, Herrlich P, Hotta H, Tanaka K, Chikuma S, Yagita H, Okumura K, Murakami M, et al. (1999). CD44 variants but not CD44s cooperate with beta1-containing integrins to permit cells to bind to osteopontin independently of arginine-glycine–aspartic acid, thereby stimulating cell motility and chemotaxis. *Cancer Res* **59**, 219–226.

[23] Senger DR and Perruzzi CA (1985). Secreted phosphoprotein markers for neoplastic transformation of human epithelial and fibroblastic cells. *Cancer Res* **45**, 5818–5823.

[24] Bramwell VH, Doig GS, Tuck AB, Wilson SM, Tonkin KS, Tomiak A, Perera F, Vandenberg TA, and Chambers AF (2006). Serial plasma osteopontin levels have prognostic value in metastatic breast cancer. *Clin Cancer Res* **12**, 3337–3343.

[25] Kramer RH and Nicolson GL (1979). Interactions of tumor cells with vascular endothelial cell monolayers: a model for metastatic invasion. *Proc Natl Acad Sci USA* **76**, 5704–5708.

[26] Folkman J (1994). Angiogenesis and breast cancer. *J Clin Oncol* **12**, 441–443.

[27] Hanahan D and Folkman J (1996). Patterns and emerging mechanisms of the angiogenic switch during tumorigenesis. *Cell* **86**, 353–364.

[28] Prols F, Loser B, and Marx M (1998). Differential expression of osteopontin, PC4, and CEC5, a novel mRNA species, during *in vitro* angiogenesis. *Exp Cell Res* **239**, 1–10.

[29] Sulzbacher I, Birner P, Trieb K, Lang S, and Chott A (2002). Expression of osteopontin and vascular endothelial growth factor in benign and malignant bone tumors. *Virchows Arch* **441**, 345–349.

[30] Fidler IJ (1990). Host and tumour factors in cancer metastasis. *Eur J Clin Invest* **20**, 481–486.

[31] Sodek J, Ganss B, and McKee MD (2000). Osteopontin. *Crit Rev Oral Biol Med* **11**, 279–303.

[32] Rosenow F, Ossig R, Thormeyer D, Gasmann P, Schluter K, Brunner G, Haier J, and Eble JA (2008). Integrins as antimetastatic targets of RGD-independent snake venom components in liver metastasis [corrected]. *Neoplasia* **10**, 168–176.

[33] O'Regan A and Berman JS (2000). Osteopontin: a key cytokine in cell-mediated and granulomatous inflammation. *Int J Exp Pathol* **81**, 373–390.

[34] He B, Mirza M, and Weber GF (2006). An osteopontin splice variant induces anchorage independence in human breast cancer cells. *Oncogene* **25**, 2192–2202.